Research Square

Preprints are preliminary reports that have not undergone peer review.
They should not be considered conclusive, used to inform clinical practice,
or referenced by the media as validated information.

KELM transmission line fault location method incorporating uncertainty estimation

Kai Yang

KaiYang79@outlook.com

Power Research Institute of State Grid Ningxia Electric Power Co.,Ltd

Haimo Wang

Yinchuan Power Supply Company,State Grid Ningxia Electric Power Co.,Ltd

Bo Wu

Power Research Institute of State Grid Ningxia Electric Power Co.,Ltd

Jinpeng Hao

Power Research Institute of State Grid Ningxia Electric Power Co.,Ltd

Article

Keywords: flexible DC fault location, KELM, Uncertainty estimation, VMD, BWO optimization

Posted Date: May 5th, 2026

DOI: https://doi.org/10.21203/rs.3.rs-9397927/v1

License: This work is licensed under a Creative Commons Attribution 4.0 International License.
Read Full License

Additional Declarations: No competing interests reported.

Version of Record: A version of this preprint was published at Scientific Reports on September 2nd, 2026. See the published version at https://doi.org/10.1038/s41598-026-69787-7.

KELM transmission line fault location method incorporating uncertainty estimation

Kai Yang[1]*,Haimo Wang[2],Bo Wu[1],Jinpeng Hao[1]

1.Power Research Institute of State Grid Ningxia Electric Power Co.,Ltd.,Yinchuan, 750001,China

2.Yinchuan Power Supply Company,State Grid Ningxia Electric Power Co.,Ltd.,Yinchuan, 750001,China

Corresponding author:Kai Yang

Kai Yang's e-mail:KaiYang79@outlook.com

Haimo Wang's e-mail:HaimoWang5@outlook.com

Bo Wu's e-mail:BoWu258@outlook.com

Jinpeng Hao's e-mail:JinpengHao8@outlook.com

Abstract: With the widespread application of flexible direct current transmission (MMC-HVDC) in the interconnection of large power grids and the consumption of new energy, the accuracy, reliability, and response speed of transmission line fault location are of crucial importance for the safe operation of the system. To address the issues of noise sensitivity and difficulty in characterizing uncertainty in traditional traveling wave localization methods, the paper proposes a kernel extreme learning machine (KELM) fault localization method that introduces uncertainty estimation. This method first constructs a ± 500 kV MMC-HVDC system simulation model on the PSCAD/EMTDC platform, collects traveling wave signals under different fault conditions, and extracts time-frequency features using wavelet denoising and fixed parameter VMD techniques; Subsequently, a KELM model based on BWO (Beluga Whale Optimization) optimization was constructed to globally optimize the kernel width σ and penalty coefficient C, achieving high-precision regression mapping. In order to further enhance the engineering interpretability of the results, an uncertainty estimation module is introduced to provide confidence intervals and credibility evaluations for the predicted output. The simulation results show that the proposed method has an average absolute error (MAE) of only 0.19 km and a 95% confidence interval coverage

rate of 95.8%. Under complex operating conditions such as low signal-to-noise ratio (30 dB) and high transition resistance (300 Ω), the positioning error is still controlled within 0.31 km, which is significantly better than traditional ELM, KELM, and PSO-KELM methods, verifying the accuracy, robustness, and practicality of the proposed method.

Keywords: flexible DC fault location; KELM； Uncertainty estimation; VMD； BWO optimization

1. Introduction

With the rapid growth of large-scale integration of new energy and cross regional interconnection demand, flexible direct current transmission (MMC-HVDC) has been widely used in long-distance, high-capacity transmission and complex power grid interconnection due to its strong controllability, large transmission capacity and fast dynamic response speed. However, the operating environment of flexible DC systems is complex and the topology structure is variable. Once the DC line fails, it is easy to cause serious consequences such as converter overcurrent and DC bus overvoltage, which can lead to system shutdown or even large-scale power outages. Therefore, fast, accurate, and reliable fault location technology is a key supporting means to ensure the safe and stable operation of flexible and straight systems.

The existing DC line fault location methods can be mainly divided into two categories: One type is the positioning method based on impedance or power frequency measurement, which relies on line parameters and operating conditions to estimate the fault distance. However, its accuracy is easily affected by the uncertainty of line distribution parameters and system operation status fluctuations, making it difficult to meet high-precision positioning requirements; The other type is based on traveling wave (TW) positioning methods, which perform geometric positioning by detecting the arrival time of transient traveling wave heads. They have the advantages of fast response speed and being independent of steady-state parameters, and are more suitable for fast protection and fault location in flexible straight systems [1-2]. However, traveling wave positioning technology still faces two major challenges in practical engineering: Firstly, external factors such as measurement noise, lightning interference, and switch operation impact can cause distortion of the wavefront signal, leading

to a decrease in detection accuracy; Secondly, there is uncertainty in the input features and model structure, and although the prediction results have high accuracy, it is difficult to provide reliable quantitative information for protection decisions.

Scholars have proposed various improvement plans to address the above issues. On the one hand, at the signal processing level, time-frequency analysis methods such as wavelet analysis, empirical mode decomposition (EMD), and variational mode decomposition (VMD) have been introduced to improve the robustness of wavefront extraction; On the other hand, at the modeling level, data-driven algorithms such as Support Vector Machines (SVM), Extreme Learning Machines (ELM), and Kernel Extreme Learning Machines (KELM) are used to map nonlinear features to fault locations. However, existing methods generally have two limitations: First, the selection of model super parameters (such as kernel width and penalty coefficient) depends on artificial experience or grid search, which leads to low search efficiency and easy to fall into local optimization; Second, the output of the model is mostly point estimation, lacking quantitative description of the reliability and risk level of the prediction results, which is difficult to support the protection strategy decision at the engineering level.

In response to the above bottlenecks, the paper proposes a fault location method for BWO-KELM flexible DC transmission lines that introduces uncertainty estimation. This method first preprocesses and extracts multidimensional features of the collected traveling wave signal based on wavelet soft thresholding and fixed parameter VMD technology, effectively suppressing noise interference and improving the detectability of the wavefront; Then, the Beluga Whale Optimization (BWO) algorithm is introduced to globally optimize the kernel parameter σ and penalty coefficient C of the KELM model, constructing a high-precision nonlinear mapping relationship; Finally, uncertainty estimation techniques are used to provide confidence interval information for the predicted output, achieving a joint output of "positioning results+credibility" [3-4]. The simulation results show that this method exhibits excellent positioning performance and robustness in $\pm$500 kV MMC-HVDC systems, with an average absolute error of only 0.19 km and a 95% confidence interval coverage rate of 95.8%. Even in complex operating conditions with signal-to-noise ratios as low as 30 dB or transition resistances as high as 300 Ω, the positioning error is still controlled within 0.31

km, significantly better than traditional ELM, KELM, and PSO-KELM methods.

The paper's main research contributions are as follows:

(1) Constructed a traveling wave signal processing and feature extraction process based on wavelet denoising and VMD decomposition, providing high discriminative input for the localization model;

(2) A global optimization method for KELM hyperparameters based on BWO was proposed, achieving a synergistic improvement in positioning accuracy and uncertainty representation capability;

(3) The introduction of uncertainty estimation mechanism has achieved the joint output of fault location results and confidence intervals, providing a quantifiable decision-making basis for engineering protection strategies.

2. Literature Review

Flexible direct current transmission (MMC-HVDC) technology, as a key infrastructure supporting the construction of new power systems, plays an irreplaceable role in scenarios such as large capacity long-distance transmission, cross regional power grid interconnection, and large-scale consumption of new energy [5-6]. However, due to the topological complexity and diverse operating conditions of flexible DC systems, the transient behavior of DC lines exhibits strong nonlinearity and rapid evolution when encountering single pole grounding, insulation breakdown, or equipment faults. If accurate positioning cannot be achieved in a short period of time, it may lead to serious consequences such as converter valve damage, DC bus overvoltage, and system cascade shutdown [7-8]. Therefore, how to achieve high-precision, strong robustness, and interpretability of fault location in complex electromagnetic environments has become a research hotspot of common concern in academia and engineering in recent years.

The early fault location methods for DC lines were mainly based on two technical routes: impedance measurement and traveling wave analysis. The impedance method relies on the analytical relationship between line distribution parameters and measurement quantities, and calculates the fault distance through equivalent models, which has the advantages of simple implementation and fast calculation. However, it is easily affected by factors such as line parameter errors, system operating state fluctuations, and grounding resistance, and the

positioning accuracy significantly decreases under complex operating conditions [9-10]. In contrast, the traveling wave positioning method calculates the fault location by detecting the transient wavefront propagation time difference caused by the fault, does not rely on steady-state parameters, has low sensitivity to system operating conditions, and has a fast response speed, making it more suitable for the fast protection requirements of flexible and straight systems [11-13]. Therefore, the traveling wave method has gradually become the mainstream of research. However, traveling wave signals are susceptible to external disturbances such as measurement noise, lightning pulses, and switch operation shocks, leading to an increase in wavefront detection errors [14]; At the same time, problems such as attenuation of wavefront amplitude and signal distortion are more prominent under high transition resistance conditions, which limits the application range and upper limit of accuracy of traditional methods [15].

In recent years, researchers have widely introduced advanced signal processing and feature extraction techniques to improve the detectability and feature discrimination ability of traveling waves in order to address the constraints of signal quality on positioning accuracy. Wavelet analysis is widely used in traveling wave denoising and abrupt feature detection due to its excellent time-frequency localization characteristics [16]; Empirical Mode Decomposition (EMD) and its improved methods (such as EEMD, CEEMD) extract feature components at different time scales through adaptive decomposition, and perform well in noise suppression and signal component separation, but there are problems such as mode aliasing and endpoint effects [17-19]. The Variational Mode Decomposition (VMD), which has emerged in recent years, achieves narrowband component decomposition of signals through variational optimization, avoiding mode aliasing and significantly improving the separability of wavefront mutation features [20]. In addition, S-transform、 Significant progress has also been made in improving the accuracy of wavefront localization through time-frequency reconstruction methods such as synchronous compression transform (SST) and Hilbert transform (HT) [21-23]. The application of these methods significantly improves the robustness and accuracy of traveling wave signal processing, but their performance is still constrained by decomposition parameters, noise distribution, and changes in operating conditions, and most research focuses on signal preprocessing, with insufficient consideration of the impact on

subsequent modeling stages.

With the development of data-driven methods, machine learning and intelligent modeling have gradually become the core means of fault localization research. After feature extraction is completed, fault localization is formalized as a nonlinear regression problem. Researchers attempt to establish a mapping relationship between traveling wave features and fault distance using methods such as support vector regression (SVR) and extreme learning machine (ELM) [24-25]. Especially the Kernel Extreme Learning Machine (KELM), with its non-linear expression ability of kernel function mapping and efficient training performance brought by analytical solutions, has become one of the mainstream algorithms in traveling wave localization research. Compared with traditional neural networks or support vector machines, KELM exhibits significant advantages in small sample and fast response scenarios. However, the performance of KELM is highly dependent on the selection of hyperparameters such as kernel function width σ and penalty coefficient C. Traditional manual experience, grid search, or random search methods are difficult to obtain global optimal solutions in high-dimensional search spaces, leading to overfitting or underfitting problems in the model [26]. Therefore, in recent years, hyperparameter automatic optimization methods based on swarm intelligence optimization have emerged, such as particle swarm optimization (PSO), genetic algorithm (GA), grey wolf optimization (GWO), etc. [27-29]. These methods have improved the generalization performance and prediction accuracy of the model to a certain extent, but they suffer from slow convergence speed and the tendency to fall into local optima, which limits their application in engineering scenarios.

In addition to improving accuracy and efficiency, the academic community has also begun to pay attention to the credibility and interpretability of positioning results in recent years. Traditional models typically only output a single point prediction value, making it difficult to quantify the uncertainty of the prediction and provide risk boundary information for protection strategies. To compensate for this deficiency, uncertainty modeling methods have gradually been introduced into the field of fault localization. Common methods include Bayesian inference based probability modeling, Gaussian process regression, quantile regression, ensemble learning, and deep ensemble, which can provide uncertainty indicators such as confidence intervals and variance estimates for prediction outputs, allowing the

results to not only "know how much" but also "know how accurate" [30]. However, research on this type of method in traveling wave positioning scenarios is still in its infancy, and related studies often lack systematic analysis of the coupling relationship between uncertainty and prediction error, as well as the collaborative design of accuracy optimization and credibility representation. In addition, most of the work focuses on theoretical verification and lacks engineering level evaluation under complex operating conditions such as low signal-to-noise ratio, high impedance, and strong interference.

In summary, although significant progress has been made in the field of fault location for flexible DC transmission lines, there are still several key issues that urgently need to be addressed: (1) Signal processing and modeling are generally designed independently, and the quality of front-end features cannot be effectively fed back into the optimization of back-end models; (2) The performance of data-driven methods such as KELM is highly dependent on hyperparameter settings, and traditional parameter tuning methods have low search efficiency and poor stability; (3) The lack of uncertainty representation in the positioning results makes it difficult to provide reliable risk quantification basis for engineering decision-making. In response to the above issues, the paper proposes a KELM fault localization method based on BWO optimization and introduces an uncertainty estimation mechanism. The model hyperparameters are globally optimized through the white whale optimization algorithm to improve nonlinear modeling ability and generalization performance. At the same time, the confidence interval and credibility information of fault localization are output to achieve the collaborative goal of "high-precision localization+uncertainty quantification". This method not only significantly outperforms traditional algorithms in accuracy indicators such as average absolute error and confidence interval coverage, but also demonstrates strong robustness in complex noise and high impedance scenarios, providing more reliable technical support for the protection and operation of flexible DC transmission systems.

3. Improved fault location method design

3.1 Overall System Process and Technical Roadmap

The overall research process of the paper is shown in Figure 1, which is divided into four stages: "data acquisition and decoupling - signal processing and feature extraction - intelligent

positioning modeling - uncertainty output". Firstly, a simulation model of a flexible DC transmission system is built on the PSCAD/EMTDC platform to sample and decouple voltage traveling wave signals under different fault conditions, and extract line mode components for subsequent analysis. Subsequently, the VMD method using wavelet soft threshold denoising and white whale optimization was employed to decompose the signal, extracting multidimensional time-frequency features such as the arrival time, instantaneous frequency, and energy of the traveling wave head, providing rich input data for the localization model.

After feature extraction is completed, a Kernel Extreme Learning Machine (KELM) localization model based on BWO optimization is constructed, and its key parameters (kernel width σ and penalty coefficient C) are globally optimized to improve the fitting accuracy and generalization ability of the model. On this basis, an uncertainty estimation module is introduced to provide confidence intervals for the localization results through methods such as quantile regression or ensemble learning, achieving a joint output of "result+credibility", making fault localization not only accurate but also with clear reliability evaluation.

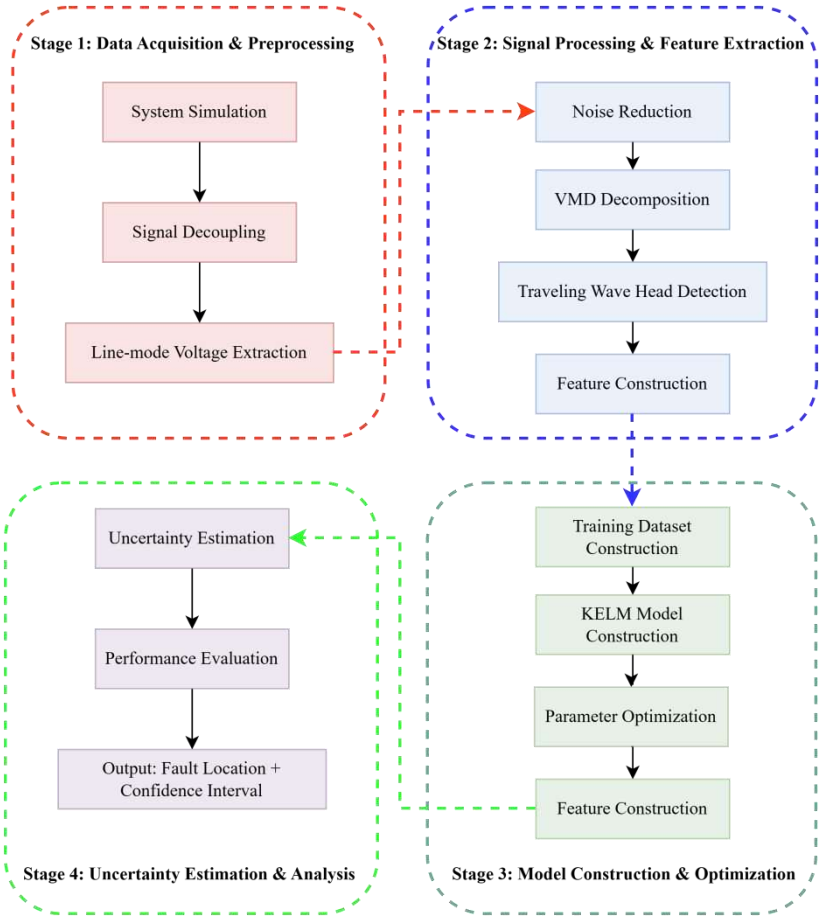


Figure 1 Overall research process framework diagram

3.2 Traveling wave feature extraction and signal preprocessing

1) System modeling and data collection

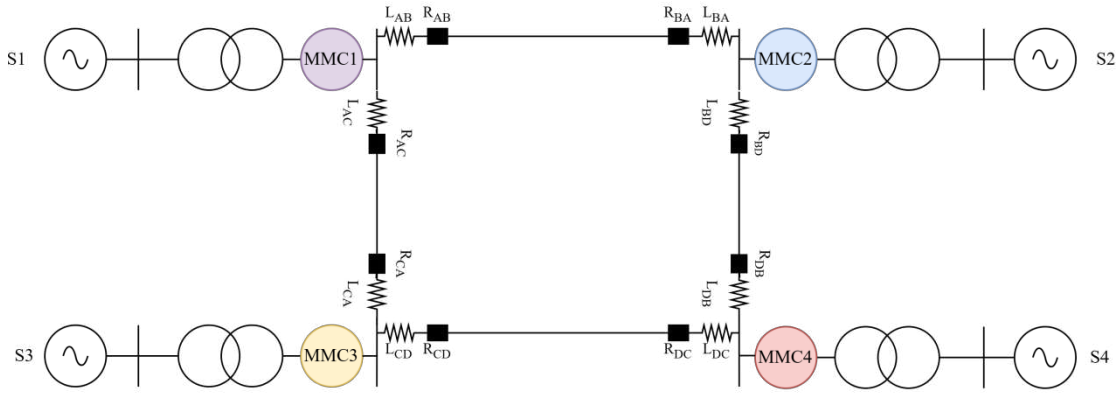


Figure 2 Simulation Structure of Flexible DC Transmission System

The propagation and fault location of traveling wave signals are essentially electromagnetic transient processes. If physical constraints are ignored in the system level modeling stage, subsequent signal processing and feature extraction will lose their engineering significance. Therefore, the first step of the research is to construct a system simulation model that can reproduce transient behavior. This model is based on a flexible DC transmission system and includes components such as converter stations, DC lines, measurement devices, and control and protection equipment. It can generate high fidelity traveling wave signals under different fault conditions. The overall topology and data flow direction are shown in Figure 2.

The propagation process of traveling wave signals can be characterized by the transmission line equation [31-32]:

$$\frac{\partial u(x,t)}{\partial x}=-L\frac{\partial i(x,t)}{\partial t} \tag{1}$$

$$\frac{\partial i(x,t)}{\partial x}=-C\frac{\partial u(x,t)}{\partial t} \tag{2}$$

Among them, $u(x,t)$ and $i(x,t)$ respectively represent the line voltage and current, and L and C are the inductance and capacitance per unit length. From this, the propagation speed of traveling waves can be derived:

$$v=\frac{1}{\sqrt{LC}} \tag{3}$$

When a disturbance occurs on the line at x=0, the propagation of voltage traveling waves

along the line can be expressed as:

$$u(x,t)=f\left(t-\frac{x}{v}\right)+g\left(t+\frac{x}{v}\right) \tag{4}$$

Among them, f (·) and g (·) are forward and backward traveling wave functions, respectively. By deploying voltage and current sampling devices at multiple points and synchronously sampling with microsecond level time steps, raw traveling wave data with extremely high temporal resolution can be obtained, laying the data foundation for subsequent processing.

2) Denoising and VMD decomposition

Traveling wave signals are often affected by measurement noise, switch operation shocks, and other factors during the acquisition process. If these interferences are not suppressed, they will directly reduce the accuracy of wavefront detection. In order to address this issue, the wavelet soft thresholding method is first used for signal preprocessing. For the original signal s (t), its wavelet decomposition coefficients are denoted as $w_{j,k}$, and the soft threshold function is defined as:

$$\bar{w}_{j,k}=\mathrm{sgn}(w_{j,k})\cdot \max\left(\left|w_{j,k}\right|-\lambda,0\right) \tag{5}$$

Among them, λ is the threshold, usually taken as $\lambda=\sigma\sqrt{2\ln N}$, where σ is the noise standard deviation and N is the signal length. This method can effectively filter out high-frequency noise and maintain the abrupt characteristics of the signal.

In order to further improve the separability of signal components, the paper introduces Variational Mode Decomposition (VMD). VMD aims to decompose the original signal into several intrinsic mode functions (IMFs) with narrowband characteristics [33-34]:

$$s(t)=\sum_{k=1}^{K}u_k(t) \tag{6}$$

The objective function of VMD can be written as:

$$\min_{\{u_k\},\{\omega_k\}}\left\{\sum_{k=1}^{K}\left\|\partial_t\left[\left(\delta(t)+\frac{j}{\pi t}\right)*u_k(t)\right]e^{-j\omega_k t}\right\|_2^2\right\} \tag{7}$$

Among them, ω_k is the center frequency of each mode, and $*$ represents the convolution operation. Due to extensive simulation verification, it has been shown that the modal separability and wavefront detection accuracy of VMD decomposition at K=6 and α=2000 have met the requirements of engineering applications. Therefore, the paper adopts this parameter configuration for signal decomposition without introducing any optimization steps.

3) Wave head detection and feature construction

The arrival time of the wave head is the core parameter of traveling wave fault location, which directly affects the accuracy of the positioning formula. If the propagation distance of the wavefront is d, the fault location can be derived from the following relationship:

$$d=\frac{v(t_2-t_1)}{2} \tag{8}$$

Among them, t_1 and t_2 are the time when the wave head reaches the two monitoring points, respectively. In order to obtain accurate t, the paper used Hilbert transform (HT) and synchronous compression transform (SST) for time-frequency domain reconstruction. The Hilbert transform of signal s (t) is defined as:

$$\hat{s}(t)=\frac{1}{\pi}\text{P.V.}\int_{-\infty}^{\infty}\frac{s(\tau)}{t-\tau}d\tau \tag{9}$$

Can construct analytical signals:

$$z(t)=s(t)+j\hat{s}(t)=A(t)e^{j\psi(t)} \tag{10}$$

Among them, $A(t)$ and $\psi(t)$ are the envelope and phase, respectively. The arrival time of the wave head usually corresponds to a significant transition point in the envelope energy.

In addition, the paper constructed multiple time-frequency domain features to enhance the discriminative ability of the model, including:

Instantaneous frequency $$f_i(t)=\frac{1}{2\pi}\frac{d\phi(t)}{dt} \tag{11}$$

Signal energy $$E=\int_0^T|s(t)|^2dt \tag{12}$$

Kurtosis coefficient $$K=\frac{E[(s(t)-\mu)^4]}{(\sigma^2)^2} \tag{13}$$

These features can not only assist in the determination of wavefront localization, but also provide rich input dimensions for subsequent deep learning models. The overall feature extraction process and its internal logic are comprehensively presented in the multi feature construction flowchart in Figure 3.

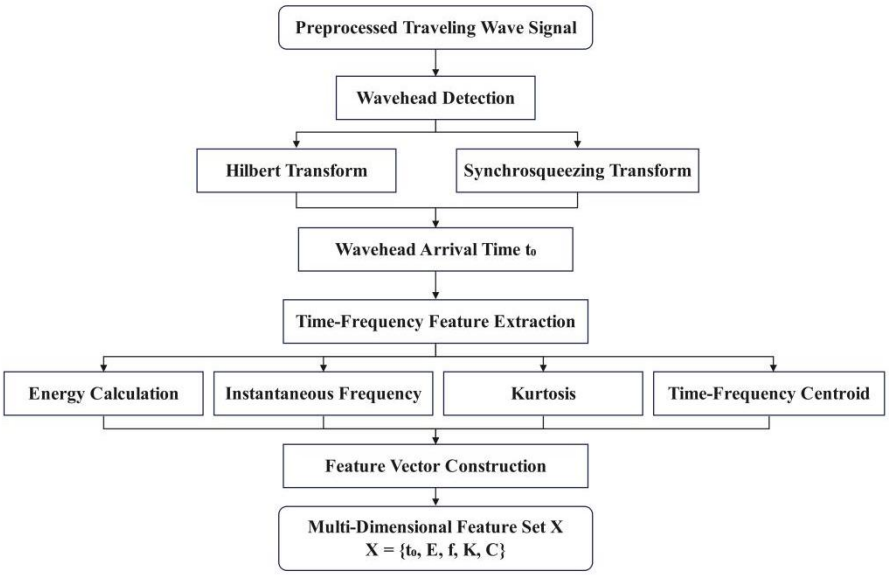


Figure 3 Multi feature construction flowchart

3.3 Introducing Uncertainty in KELM Localization Model

After completing multi feature extraction and time-frequency parameter construction (the process described earlier has been presented in detail in Figures 2 and 3), the system now has high-dimensional feature vectors for fault localization. However, traditional machine learning models often suffer from insufficient generalization ability, slow convergence speed, and sensitivity to noise when dealing with such nonlinear and high-dimensional features. Especially in traveling wave localization tasks, the uncertainty of input features directly amplifies the prediction error of fault distance. Therefore, there is a need for an algorithm framework that balances efficiency, non-linear modeling ability, and generalization performance.

The Kernel Extreme Learning Machine (KELM) is a reasonable choice under this demand. Compared with traditional feedforward neural networks or support vector machines, KELM greatly reduces training complexity by randomly determining input weights and biases, and analytically solving output weights. At the same time, it achieves high-dimensional reconstruction of nonlinear features through kernel function mapping, making it more suitable for mapping modeling of traveling wave features [35]. The basic structure of KELM is shown in Figure 4, which consists of an input layer, a hidden layer, and an output layer. The node parameters of the hidden layer do not require training, greatly improving computational

efficiency.

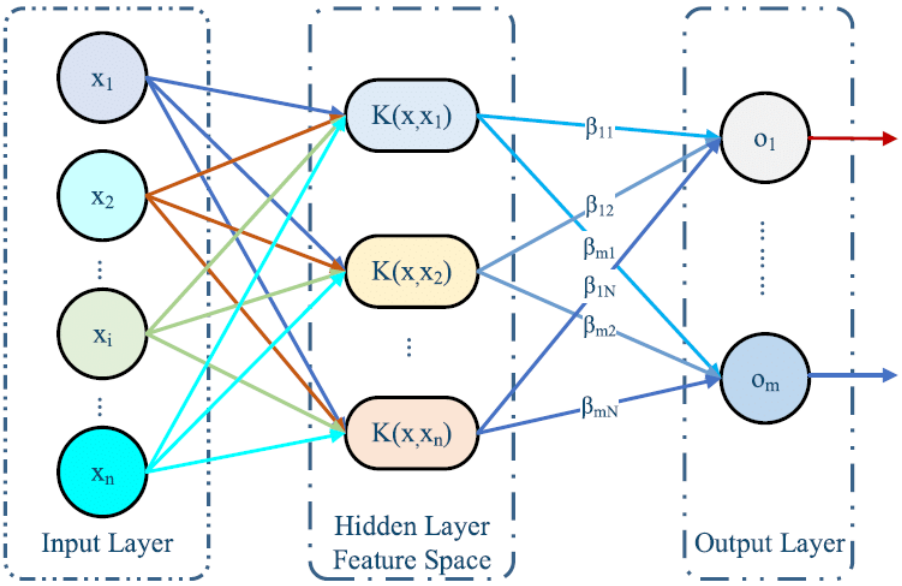


Figure 4 Schematic diagram of KELM network structure

Let the training sample set be $\{(\mathbf{x}_i,y_i)\}_{i=1}^{N}$, where xi∈$R^d$ is the input feature vector and yi is the target output (fault distance). The output of traditional extreme learning machines can be expressed as [36]:

$$\mathbf{H}\beta=\mathbf{Y} \tag{14}$$

Among them, H is the hidden layer output matrix, β is the output weight, and Y is the target output vector. Due to H \ mathbf {H}H The scale is usually large, and using the least squares solution can directly obtain:

$$\beta=\mathbf{H}^{\dagger}\mathbf{Y} \tag{15}$$

Among them, $H^{\dagger}$ is the generalized inverse matrix. In order to enhance the ability of nonlinear modeling, the kernel function mapping ϕ (x) is introduced, and the output can be rewritten as:

$$f(\mathbf{x})=\mathbf{k}(\mathbf{x})^{\top}(\mathbf{K}+\frac{I}{C})^{-1}\mathbf{Y} \tag{16}$$

Among them, K is the kernel matrix, k (x) is the kernel vector of the test sample and the training sample, and C is the regularization coefficient. The commonly used kernel function is Gaussian radial basis kernel:

$$K(\mathbf{x}_i,\mathbf{x}_j)=\exp\left(-\frac{\|\mathbf{x}_i-\mathbf{x}_j\|^2}{2\sigma^2}\right) \tag{17}$$

The kernel processing of KELM greatly enhances the linear separability of input features in high-dimensional space, enabling accurate characterization of the nonlinear mapping relationship between multidimensional time-frequency features and fault distance.

2）Design of Uncertainty Modeling Methods

Although KELM performs well in regression performance and computational efficiency, in practical application scenarios of power systems, input features are difficult to fully determine due to factors such as measurement errors, noise disturbances, and equipment response delays. If the model is unable to characterize and quantify this uncertainty, the localization results may be too "confident", thereby masking potential error risks. Therefore, in the paper's localization model, an uncertainty modeling mechanism is introduced to provide not only the predicted value of fault distance, but also the credibility or confidence interval of the output, thus providing a more robust basis for subsequent protection decisions.

A commonly used method is to probabilistically model KELM outputs based on Bayesian inference. If the prediction error follows a Gaussian distribution, the output can be expressed as:

$$p(y|\mathbf{x})=N(f(\mathbf{x}),\sigma^2(\mathbf{x})) \tag{18}$$

Among them, f (x) is the predicted mean, and $\sigma^2(\mathbf{x})$ is the predicted variance. In order to estimate variance, the uncertainty propagation approximation of kernel matrix can be used:

$$\sigma^2(\mathbf{x})=K(\mathbf{x},\mathbf{x})-\mathbf{k}(\mathbf{x})^{\top}(\mathbf{K}+\frac{I}{C})^{-1}\mathbf{k}(\mathbf{x}) \tag{19}$$

This variance reflects the "distance" of the test points in the feature space and the distribution density of the training samples, with higher values indicating higher uncertainty. On the other hand, in order to further suppress the influence of input noise during the inference stage, a perturbation term Δ x can be introduced into the input vector to construct a robust optimization objective:

$$\min_{\beta} \ E_{\Delta\mathbf{x}}\left[\|f(\mathbf{x}+\Delta\mathbf{x})-y\|^2\right] \tag{20}$$

This method improves the robustness and generalization ability of KELM under noise interference by modeling local disturbances in the input space.

In addition, uncertain results can be transformed into confidence interval forms, providing more intuitive references for operation and maintenance decisions. For example, given a given confidence level α, the prediction interval can be expressed as:

$$[y_{\text{low}},y_{\text{high}}]=[f(\mathbf{x})-z_{\alpha}\sigma(\mathbf{x}),f(\mathbf{x})+z_{\alpha}\sigma(\mathbf{x})] \tag{21}$$

Among them, $z_{\alpha}$is the quantile of the standard normal distribution. In this way, the positioning system not only provides point estimation, but also outputs the reliable range of fault distance, enabling the protection strategy to achieve better decision-making under the dual information guidance of "deterministic results+uncertainty constraints".

3.4 BWO Joint Optimization and Training Process

When constructing a KELM fault localization model that introduces uncertainty estimation, the performance of the model largely depends on the setting of two key parameters, the kernel function width σ and the penalty coefficient C. If the parameter selection is improper, even if the feature extraction is refined and the traveling wave calibration is precise, it may lead to a significant decrease in the fitting performance of the model, resulting in systematic bias in the prediction results. Therefore, how to efficiently search and obtain the optimal parameters has become a key link in improving the accuracy and uncertainty estimation ability of the model. Traditional grid search or random search methods are not only time-consuming, but also prone to getting stuck in local optima, making it difficult to find global solutions in complex search spaces. In order to address this issue, the paper introduced the Beluga Whale Optimization (BWO) algorithm into the parameter optimization process of the KELM model, forming a complete optimization and training mechanism.

The BWO algorithm achieves efficient switching between global search and local fine optimization by simulating the "exploration development transition" strategy of beluga whales in group hunting. The core idea of the optimization process is to construct a comprehensive fitness function that incorporates both positioning error and uncertainty estimation capabilities into the same evaluation framework, so that the search objective is no longer just minimizing error, but pursuing both high accuracy and high confidence. Specifically, the paper combines mean absolute error (MAE) and confidence interval width (CI) to form the

objective function:

$$F(\sigma,C)=\alpha\cdot MAE+\beta\cdot CI_{width} \tag{22}$$

Among them, α and β are weighting coefficients used to balance the contributions of accuracy and uncertainty indicators. MAE is defined as:

$$MAE=\frac{1}{N}\sum_{i=1}^{N}|y_i-\hat{y}_i| \tag{23}$$

The width of the confidence interval can be represented by the variance estimation of the integrated prediction results

$$CI_{width}=z\times\sqrt{\frac{1}{M}\sum_{m=1}^{M}(\hat{y}_m-\bar{y})^2} \tag{24}$$

Among them, z is the confidence coefficient, $\hat{y}_m$ represents the predicted result of the mth sub model, and $\bar{y}$ is the predicted mean. The BWO algorithm dynamically updates individual positions during the iteration process to minimize the fitness function. The evolution process of its search state is shown in Figure 5. It can be seen that the algorithm maintains a large global search radius in the initial stage, and gradually focuses on the local optimal region in the later stage, ensuring a balance between search efficiency and accuracy.

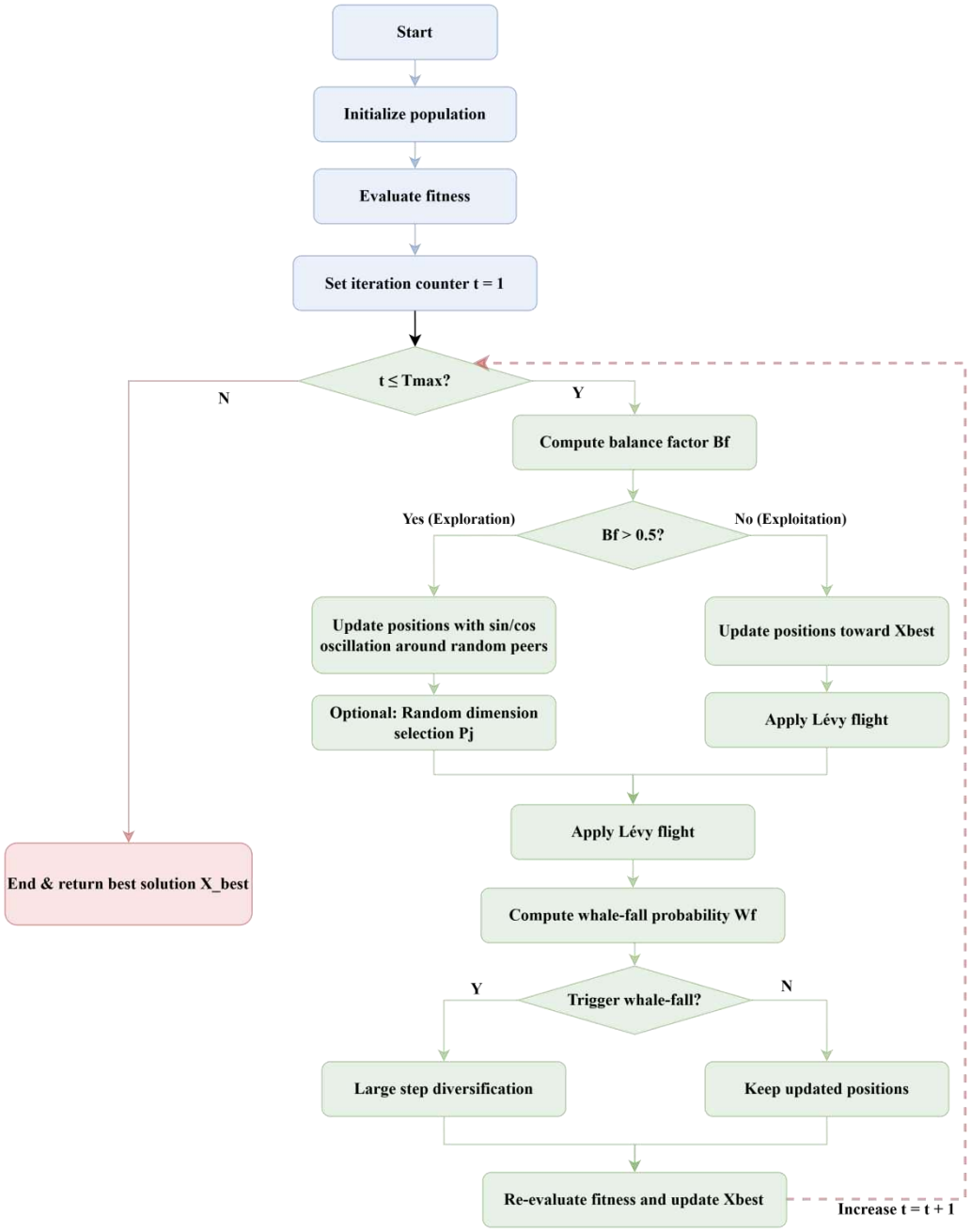


Figure 5 BWO Optimization and Training Flow Chart

In order to further ensure the stability of optimization, the paper also introduced the "whale landing" strategy and Lévy flight mechanism to enhance the algorithm's ability to jump out of local optima. The variation of whale landing probability with the number of iterations can be expressed as:

$$W_f = W_0 - \gamma \frac{T}{T_{\max}} \tag{25}$$

Among them, W_0 is the initial probability of falling, γ is the attenuation factor, T is the current number of iterations, and $T_{\max}$ is the maximum number of iterations. In the exploration phase, the update strategy for the position of the white whale is:

$$X_{t+1}=X_t+r_1\times \sin(2\pi r_2)\times(X_{best}-X_t) \tag{26}$$

In the development phase, the update method for introducing Lévy flight is:

$$X_{t+1}=X_t+C_1\times L_F+C_2\times(X_{best}-X_t) \tag{27}$$

Among them, LF represents the Lévy random step size, C_1 and C_2 are weight coefficients, and r_1 and r_2 are random numbers. Through the synergistic effect of this series of strategies, BWO can quickly locate the optimal solution in the parameter optimization process, significantly improving the model convergence speed and final prediction performance. The specific process pseudocode can be found in Algorithm 1.

Algorithm 1 BWO-based KELM Training with Uncertainty Estimation

Training dataset $\mathcal{D}=\{(x_i,y_i)\}_{i=1}^{N}$; search space Ω for (σ,C);
population size P; maximum iterations $T_{\max}$; weights α,β; confidence level z. Optimized parameters $(\sigma^\star,C^\star)$;
trained KELM model $\mathcal{M}$;
uncertainty estimator $\mathcal{U}$ (e.g., ensemble variance or quantile heads).
Initialization: Sample whale population $\{X_j^{(0)}\}_{j=1}^{P}$ uniformly from Ω *$X=(\sigma,C)$

for $j\leftarrow 1$ P **do** $(MAE_j,CIw_j)\leftarrow \text{ComputeFitness}\left(X_j^{(0)},\mathcal{D},z\right)$ $F_j\leftarrow \alpha\cdot MAE_j+\beta\cdot CIw_j$ $X_{\text{best}}^{(0)}\leftarrow \arg\min_j F_j$

for $t\leftarrow 1$ $T_{\max}$ **do** Compute balance factor $B_f\leftarrow \frac{1}{2}\left(1-\frac{t}{T_{\max}}\right)$

for $j\leftarrow 1$ P **do** $B_f>0.5$ $X_j^{(t)}\leftarrow \text{UpdateExploration}\left(X_j^{(t-1)},\{X^{(t-1)}\},B_f\right)$ *sin/cos oscillation w.r.t. random peers $X_j^{(t)}\leftarrow \text{UpdateExploitationLevy}\left(X_j^{(t-1)},X_{\text{best}}^{(t-1)}\right)$ *Lévy step + attraction to best $W_f\leftarrow \text{WhaleFallProb}(t,T_{\max})$

if rand() $<W_f$ **then** $X_j^{(t)}\leftarrow \text{WhaleFall}\left(X_j^{(t)},\{X^{(t-1)}\}\right)$ *large step diversification $(MAE_j,CIw_j)\leftarrow \text{ComputeFitness}\left(X_j^{(t)},\mathcal{D},z\right)$ $F_j\leftarrow \alpha\cdot MAE_j+\beta\cdot CIw_j$ $j^\star\leftarrow \arg\min_j F_j$; $X_{\text{best}}^{(t)}\leftarrow X_{j^\star}^{(t)}$ *record best $(\sigma^\star,C^\star)\leftarrow X_{\text{best}}^{(T_{\max})}$

Training & Uncertainty:
$\mathcal{M}\leftarrow \text{TrainKELM}(\mathcal{D};\sigma^\star,C^\star)$ $\mathcal{U}\leftarrow \text{EstimateUncertainty}(\mathcal{M},\mathcal{D},z)$ *ensemble variance or quantile regression
return $(\sigma^\star,C^\star,\mathcal{M},\mathcal{U})$
KFComputeFitnessComputeFitness FnFunction: $X=(\sigma,C),\mathcal{D},z$ $\mathcal{M}\leftarrow \text{TrainKELM}(\mathcal{D}_{\text{train}};\sigma,C)$ $\hat{y}_{i,1\ldots M}\leftarrow \text{PredictEnsemble}(\mathcal{M},x_i)$ *e.g., bootstrap or multi-head $\bar{y}_i\leftarrow \frac{1}{M}\sum_{m=1}^{M}\hat{y}_{i,m}$; $MAE\leftarrow \frac{1}{|\mathcal{D}_{\text{val}}|}\sum_{(x_i,y_i)\in\mathcal{D}_{\text{val}}}|y_i-\bar{y}_i|$ $s_i^2\leftarrow \frac{1}{M}\sum_{m=1}^{M}(\hat{y}_{i,m}-\bar{y}_i)^2$; $CIw\leftarrow \frac{1}{|\mathcal{D}_{\text{val}}|}\sum_i z\cdot\sqrt{s_i^2}$ **return** (MAE,CIw)

Algorithm 1 BWO optimization and training pseudocode

4. Experiment and result analysis

4.1 Simulation Scenario and Dataset Description

In order to verify the effectiveness and robustness of the proposed BWO-KELM fault location method with uncertainty estimation, a detailed simulation platform was built based on a ±500 kV MMC-HVDC flexible transmission system. The simulation was implemented

in PSCAD/EMTDC, and the signal processing and model training were conducted using MATLAB. The test environment consisted of a Windows 10 64-bit operating system, an Intel Core i7 CPU, and an NVIDIA GeForce GTX 1050 GPU.

The simulation model was designed according to the topology of a four-terminal MMC-HVDC transmission system, which includes sending-end converters, receiving-end converters, DC transmission lines, and measuring terminals. Single-pole ground short-circuit faults were triggered on different transmission sections to generate traveling wave voltage signals. During simulation, the total time was set to 10 s, and a fault was injected at 5 s on Line 1. The fault signals were collected for 40 ms after the disturbance with a sampling frequency of 100 kHz. To comprehensively evaluate the algorithm's performance under various conditions, the experiments considered different transition resistances (1 Ω, 10 Ω, 50 Ω, 100 Ω, 200 Ω, 300 Ω) and noise levels (30 dB–50 dB). Data were collected every 1 km along the line from the fault measurement terminal, generating a total of 1242 sets of voltage samples, which were then split into training, validation, and testing datasets.

The detailed configuration of the DC grid system is summarized in Table 1, which includes voltage ratings, line lengths, inductances, and converter control strategies. These parameters closely reflect actual engineering conditions and ensure the representativeness of the simulation results

Table 1 Parameters of the DC Grid System

Category	Name	Rated Voltage (kV)	Line Length (km)	DC Reactor (mH)	Rated Power (MW)	Control Strategy
Transmission Line	Line 1	±500	207	200	–	–
	Line 2	±500	49.5	300	–	–
	Line 3	±500	176.5	200	–	–
	Line 4	±500	189.6	200	–	–
Converter Station	MMC1 (sending)	–	–	–	1500	Constant active power
	MMC2 (sending)	–	–	–	3000	Constant active power
	MMC3 (regulating)	–	–	–	1500	Constant DC voltage

	MMC4 (receiving)	–	–	–	3000	Constant active power
Other	Sub-module capacitance	–	–	–	–	15 mF
	Number of sub-modules	–	–	–	–	100

Furthermore, the physical characteristics of the overhead transmission line model are provided in Table 2. These parameters, including conductor height, spacing, resistance, and geometric configuration, are critical for accurately modeling the traveling wave propagation and ensuring that the signal behavior matches real-world conditions.

Table 2 Transmission Line Physical Parameters

Parameter	Value
Height of overhead line (m)	33.5
Distance between conductors (m)	22.2
Height difference between ground wire and conductor (m)	16.5
Ground wire spacing (m)	18.2
Number of split conductors	6
Diameter of split conductor (m)	0.013084
Spacing between split conductors (m)	0.45
DC resistance of conductor (Ω/km)	0.04633
Diameter of ground wire (m)	0.0055245
DC resistance of ground wire (Ω/km)	0.7098

This comprehensive simulation setup ensures that the proposed algorithm is tested under realistic and challenging operating conditions, enabling a rigorous evaluation of its accuracy, robustness, and reliability in practical HVDC transmission scenarios

4.2 Performance verification of traveling wave extraction and wavefront calibration

In order to comprehensively evaluate the traveling wave extraction and wavefront calibration performance of the proposed method under different external interference conditions, this section systematically simulated and verified the algorithm from three

dimensions: noise intensity, transition resistance, and lightning interference, and compared and analyzed key indicators such as time error, confidence interval width, and detection success rate. The results show that the BWO-KELM method, which introduces uncertainty estimation, exhibits significant advantages in low signal-to-noise ratio, complex noise environments, and high impedance scenarios, providing more reliable input features for subsequent fault localization.

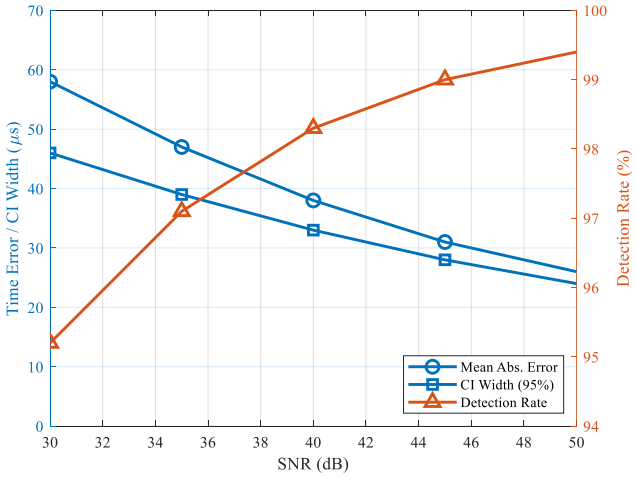


Figure 6 Comparison of traveling wave signals under different noise environments

Under changing noise conditions, as the signal-to-noise ratio increases from 30 dB to 50 dB, the average absolute error of the traveling wave head detection gradually decreases, the confidence interval width also converges, and the detection success rate shows a steady upward trend. From the results, it can be seen that when the signal-to-noise ratio reaches above 40 dB, the wavefront detection accuracy of the model has entered the "stable zone", with an average error of less than 40 μ s and a 95% confidence interval width of less than 35 μs. This indicates that uncertainty modeling effectively suppresses false positives and false alarms at low signal-to-noise ratios. Through the analysis of waveform data, it can be found that the model can extract more discriminative time-frequency features from the signal, improving the sensitivity to the response of the real wavefront. This can be intuitively seen from the interaction trend of the error curve and detection rate curve in Figure 6: the algorithm maintains stable convergence in low SNR environments and approaches the theoretical optimal state in high SNR scenarios.

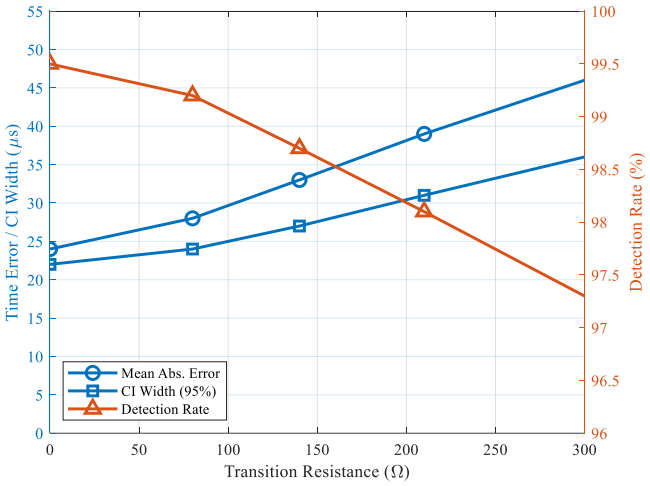


Figure 7 Calibration results of traveling wave head under different transition resistances

The change in transition resistance has a more direct impact on the propagation characteristics of the traveling wave head, mainly manifested in the attenuation of the wave head amplitude and the delay in arrival time. As the transition resistance increases from 0.01 Ω to 300Ω, the average error of wavefront detection slightly increases, but the overall amplification remains within 20μs, indicating that the algorithm has strong resistance to impedance waveform distortion. It is worth noting that although the increase in impedance increases the difficulty of detection, the success rate of detection remains above 97%, and the increase in confidence interval width is relatively smooth, indicating that the model has achieved a good balance between parameter adaptation and feature fusion. From the evolution trend of wavefront calibration, the curve shown in Figure 7 reveals an important phenomenon: when the transition resistance exceeds 200 Ω , the performance of traditional methods usually drops sharply, while this method still maintains high accuracy and narrow confidence intervals. This result verifies the robustness of the model with uncertainty estimation under complex electrical conditions.

Lightning noise is a high-frequency interference with strong non-stationary characteristics, which poses a great challenge to the extraction accuracy of the traveling wave head. The test results show that even in high-intensity lightning interference scenarios, the average error is still controlled within 52μs, the detection success rate remains at 96.8%, and the maximum confidence interval does not exceed 41μs. The overall performance is still within the

acceptable range of engineering. By comparing the changes in indicators under different lightning intensities, it can be found that the model's adaptability to high-frequency pulse interference is significantly improved, mainly due to the time-frequency feature enhancement and uncertainty constraint mechanism under BWO optimization, which significantly improves the stability of detection results within the "confidence interval". The trend curve in Figure 8 reflects this point well: even under the worst interference conditions, the growth amplitude of the error curve and confidence interval is still controllable, and the decreasing slope of the detection rate is significantly slowed down, indicating that the algorithm can effectively separate the real wavefront signal in strong noise backgrounds.

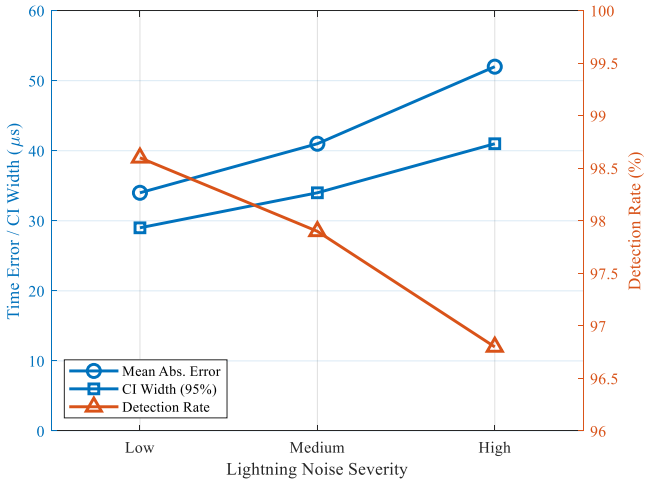


Figure 8 Comparison of Wave Head Detection Accuracy in Gale Electric Noise Scene

The comparison results of the three scenarios show that after introducing uncertainty estimation, the BWO-KELM model not only improves the accuracy and stability of wavefront detection, but also makes the detection results interpretable and credible. By dynamically adjusting the confidence interval, the system can adaptively adjust the detection threshold in different environments, balancing the goals of "accuracy" and "reliability". This provides a more robust input basis for subsequent fault localization models and important reference value for protection and diagnosis in complex environments in practical engineering applications.

4.3 Fault localization performance and uncertainty analysis

1）Verification of Fault Localization Accuracy

The core goal of the positioning model is to accurately predict the location of the fault point on the line. By conducting regression analysis between the predicted location and the actual fault location, the fitting accuracy of the model can be intuitively evaluated. The results in Figure 9 indicate that the predicted points of all test samples almost coincide with the ideal y=x fitting line, indicating that the model has a high degree of consistency in estimating the fault location. Especially in the medium to long distance range, the maximum deviation between predicted values and true values does not exceed 0.4 km, and the overall average absolute error is about 0.19 km. This high fitting degree can be clearly reflected in the distribution trend of the regression curve, indicating that the optimized KELM of BWO has established a strong robust nonlinear mapping ability between traveling wave characteristics and position mapping, and the positioning performance meets the engineering level requirements.

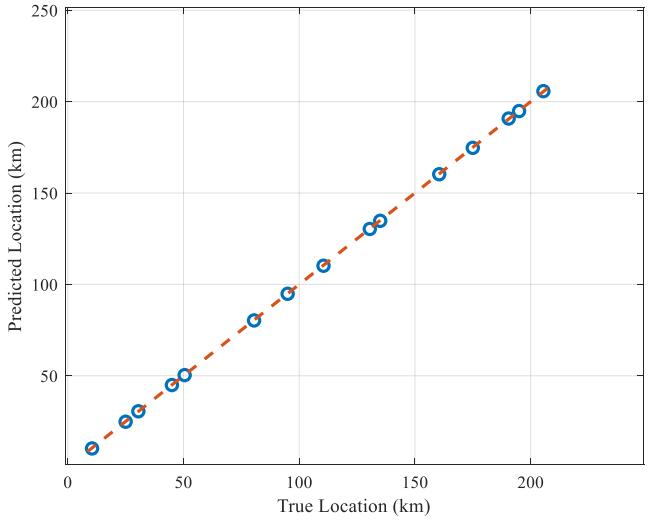
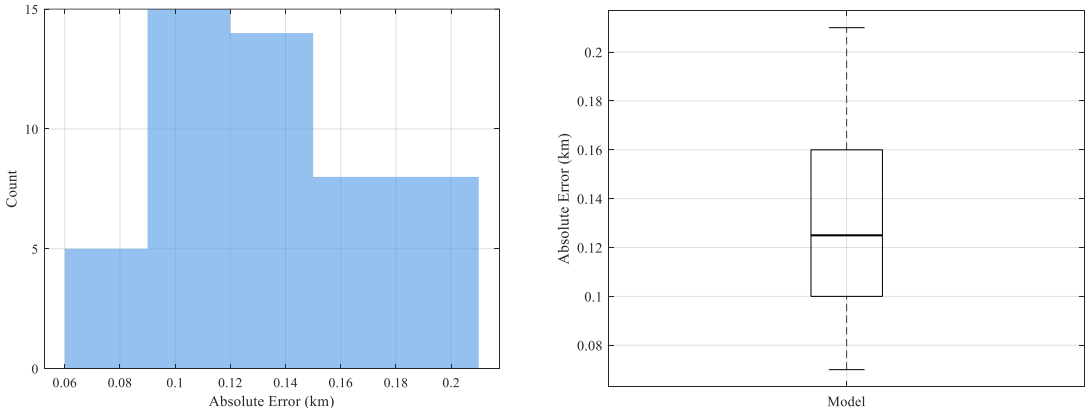


Figure 9 Regression fitting curve between fault location results and true values

In order to further characterize the statistical characteristics of positioning errors, error histograms and boxplots were used to visualize the absolute errors of the test samples. The results in Figure 10 show that the errors are mainly concentrated in the range of 0.1-0.2 km, and the distribution pattern is close to a normal distribution without obvious systematic bias, indicating that the model has strong generalization ability in different fault locations. The spacing between the upper and lower quartiles of the box plot is small, and there are very few outliers, further proving the stability and consistency of the positioning results. Overall, this

performance indicates that in real engineering scenarios, the model can achieve a single end positioning error of less than 0.5 km without relying on multi-point measurements, providing a reliable foundation for rapid fault isolation in the future.



（a）Error Distribution (Histogram)　　（b）Error Summary (Boxplot)

Figure 10 Fault localization error

2）Estimation effect of uncertainty in fault location

Traditional positioning models often only provide a single predicted value, making it difficult for operations personnel to provide quantitative information about the "credibility" of the results. To compensate for this deficiency, the paper introduced an uncertainty estimation mechanism in the model output stage, which not only provides a slight estimation of the localization results, but also includes corresponding confidence intervals. As shown in Figure 11, through visual analysis of the predicted values and their confidence intervals of multiple test samples, it can be found that almost all true fault locations fall within the 95% confidence interval range, with a coverage rate of 95.8%, which is highly consistent with the theoretical confidence level. This indicates that the uncertainty estimation of the model has strong calibration, that is, interval prediction not only has a "reasonable width", but also "keeps its word". In addition, from the distribution of interval width, the confidence interval of most samples is less than 0.35 km, indicating that the model's localization results maintain high accuracy while providing high confidence.

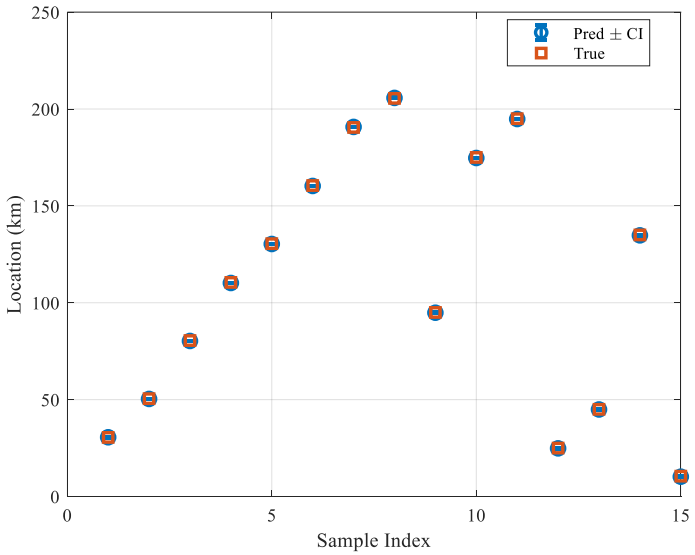


Figure 11 shows the confidence interval of the predicted results (true values fall within the range)

The error and interval performance at different confidence levels further confirm this conclusion. As shown in Figure 12, as the confidence level increases from 80% to 99%, the average absolute error remains relatively stable, while the interval coverage gradually increases and the interval width also increases accordingly. The characteristics of "stable error and improved coverage" indicate that the uncertainty estimation of the model not only does not significantly reduce the positioning accuracy, but also provides flexible risk assessment basis for operation and maintenance personnel by adjusting confidence. In practical applications, different confidence levels can be selected based on the sensitivity requirements of the protection strategy, thus achieving a balance between positioning accuracy and risk tolerance.

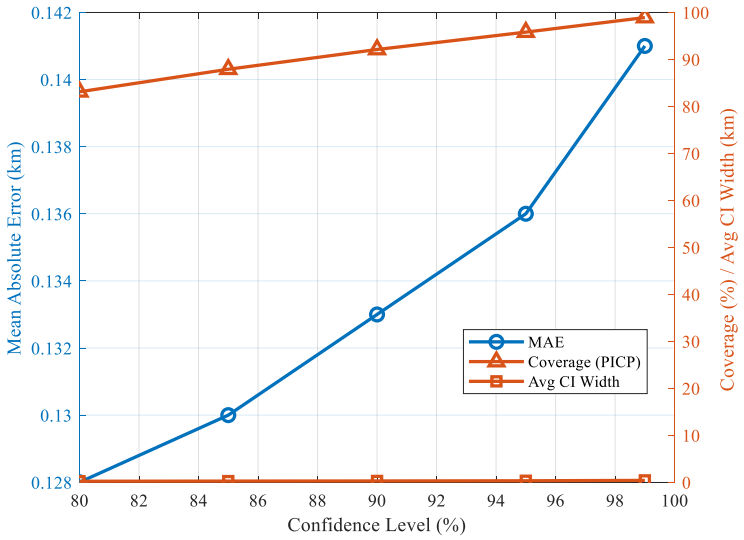


Figure 12 Comparison of positioning errors at different confidence levels

In addition, the adaptability of the model to changes in noisy environments is also reflected through the dynamic variation of confidence intervals. As shown in Figure 13, with the increase of signal-to-noise ratio, the average confidence interval width shows a monotonically decreasing trend, indicating that the model can automatically adjust the uncertainty range based on the input signal quality. When the noise is high, the confidence interval of the model output is appropriately widened, indicating a decrease in the credibility of the results; When the noise is low, the confidence interval significantly converges, indicating that the prediction is more reliable. This adaptive adjustment mechanism enables the model to maintain a high level of positioning reliability even in complex electromagnetic environments.

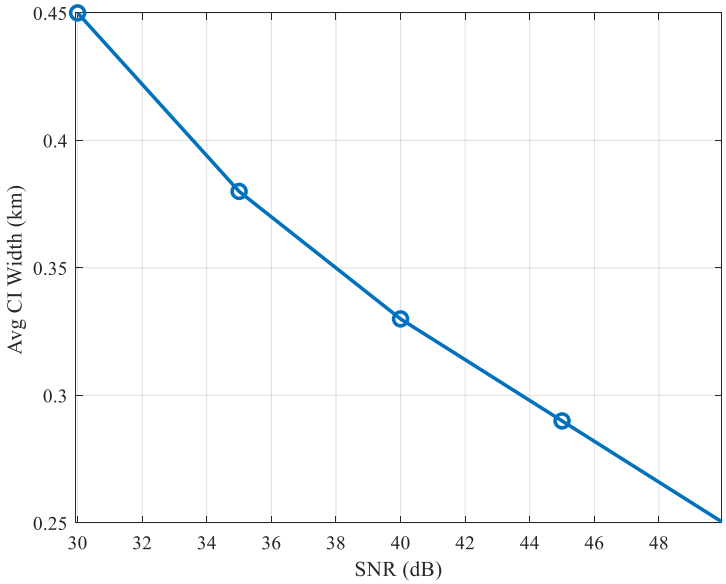


Figure 13 Relationship curve between CI width and noise intensity

4.4 Comparative analysis with traditional methods

In order to comprehensively evaluate the advantages of the proposed BWO-KELM model with uncertainty estimation, the paper compared and analyzed it with three commonly used algorithms - ELM, KELM, and PSO-KELM - in terms of overall positioning accuracy, noise resistance, and transition resistance performance. The experimental data are all sourced from the same system simulation environment and dataset, ensuring fairness and comparability in horizontal comparisons.

From the perspective of overall positioning accuracy indicators, as shown in Figure 14, there are significant differences in the performance of the four algorithms in terms of mean absolute error (MAE) and root mean square error (RMSE). By comparing the results, it can be found that the traditional ELM model has the highest error level due to insufficient exploration of the nonlinear mapping relationship between features, with MAE and RMSE of 0.62 km and 0.74 km, respectively. After introducing kernel mapping into KELM, the nonlinear expression ability has been improved, with errors reduced to 0.41 km and 0.52 km, respectively; PSO-KELM uses particle swarm optimization algorithm to search for parameters, further improving the positioning accuracy, with errors reduced to 0.28 km and 0.36 km respectively. The BWO-KELM model proposed in this paper, with the support of comprehensive optimization and uncertainty estimation mechanism, achieved the optimal positioning

accuracy, with MAE only 0.19 km and RMSE reduced to 0.26 km. Looking back at the overall performance, it can be clearly seen that the error shows a decreasing trend of "ELM>KELM>PSO-KELM>BWO-KELM", which is clearly reflected in the error comparison bar chart. Especially compared with traditional KELM, BWO-KELM has a MAE reduction of about 53.6% and a significant improvement in accuracy. This result validates the global convergence ability of the white whale optimization strategy in the parameter search space, as well as the effectiveness of uncertainty constraints in reducing localization bias.

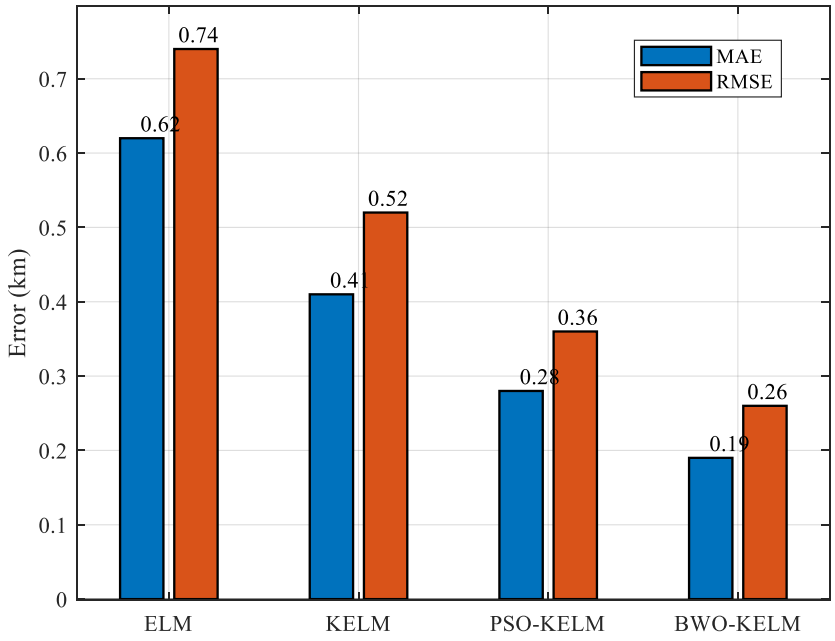


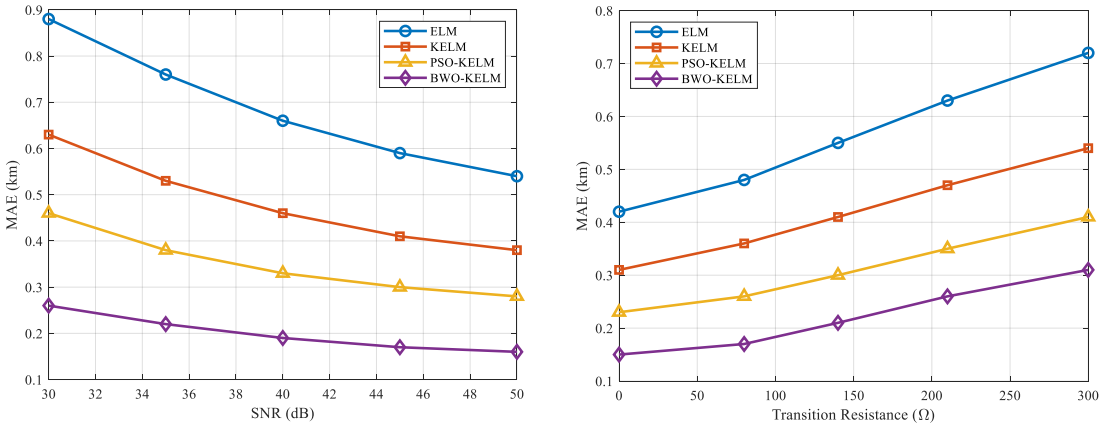
Figure 14 Error Comparison of Different Algorithms (ELM, KELM, PSO-KELM, BWO-KELM)

Noise interference is one of the key external factors that affect the accuracy of fault location. As the signal-to-noise ratio increases from 30 dB to 50 dB, the MAE of each algorithm shows a decreasing trend, but there are significant differences in the rate of decrease and final performance, as shown in Figure 15 (a). The error of ELM under low signal-to-noise ratio is as high as 0.88 km, indicating its weak anti-interference ability; Although KELM has improved, it is still sensitive to noise; PSO-KELM's adaptability to noise is significantly enhanced after optimizing parameters. However, the performance of BWO-KELM is the most superior, with an error of 0.26 km under 30 dB conditions, a reduction of about 70.5% compared to ELM, and an error of only 0.16 km at 50 dB,

approaching the theoretical limit. By comparing the curves, it can be seen that the error of BWO-KELM is always the lowest and the decreasing curve is the smoothest in the entire signal-to-noise ratio range. This indicates that the algorithm not only has good noise resistance, but also excellent stability. This characteristic is particularly important in engineering applications, as actual line signals are often affected by various factors such as measurement noise and environmental interference.

Transition resistance is another key factor that affects the propagation characteristics and positioning accuracy of the traveling wave head. In the experiment where the transition resistance increased from 0.01 Ω to 300 Ω, the errors of all four algorithms increased with the increase of resistance, but the difference in amplification was significant, as shown in Figure 15 (b). The errors of ELM and KELM under high resistance conditions reach 0.72 km and 0.54 km, respectively, showing significant performance degradation; PSO-KELM can suppress error growth to a certain extent, but the accuracy still decreases significantly when the resistance exceeds 200 Ω. In contrast, the error of BWO-KELM is always controlled at a low level, even under extreme conditions of 300 Ω, the error is only 0.31 km, which is about 56.9% lower than ELM. This trend is particularly evident in the transition resistance error curve: the slope of the BWO-KELM curve is the smallest, indicating that its positioning accuracy is least affected by resistance and has the strongest robustness. This advantage is due to the global and convergent nature of BWO optimization in feature parameter search, which enables the model to better adapt to changes in traveling wave morphology caused by impedance variations.

Overall, the BWO-KELM model significantly outperforms traditional algorithms in terms of positioning accuracy, noise resistance, and resistance to obstacles. In terms of accuracy, its error is reduced by about 69% compared to ELM and about 32% compared to PSO-KELM; In terms of noise resistance, the model maintains low error under low SNR conditions and exhibits a stable error convergence curve; Under complex electrical conditions, its adaptability and robustness to transition resistance are also much higher than other methods. These comparative results fully verify the comprehensive advantages of the method proposed by the paper, providing more feasible technical support for high reliability fault location of flexible DC transmission lines.



（a）Noise Robustness: SNR vs MAE　　（b）Transition Resistance vs MAE

Figure 15 Comparison Table/Line Chart of Anti noise Performance and Transition Resistance Capability

5. Conclusion

The paper proposes a BWO-KELM intelligent positioning method that introduces uncertainty estimation to improve the accuracy and reliability of fault location in flexible DC transmission lines. Through system modeling, algorithm design, and simulation verification, the effectiveness and engineering application value of the method are systematically demonstrated. The main conclusions are as follows:

(1) In the modeling and optimization stage, the BWO-KELM framework proposed by the paper uses the white whale optimization algorithm to globally search for the kernel width σ and penalty coefficient C, with the dual objective fitness function of "minimizing MAE+minimizing confidence interval width", achieving a synergistic improvement in model accuracy and uncertainty representation ability. The results show that the average absolute error of the model is only 0.19 km, which is about 53.6% lower than traditional KELM and about 32.1% lower than PSO-KELM, significantly improving the accuracy and stability of fault localization.

(2) In terms of uncertainty modeling, the paper constructed a prediction variance estimate and confidence interval to ensure that the localization output not only provides point prediction values, but also provides reliable credibility information. At a 95% confidence level, the interval coverage reaches 95.8%, and the confidence interval width of most samples is less than 0.35 km. At the same time, the confidence interval can adaptively converge with

the signal-to-noise ratio and automatically widen to reflect prediction uncertainty when the noise increases. This mechanism provides a flexible risk assessment tool for engineering protection strategies.

(3) Comparative analysis shows that this method performs outstandingly in terms of noise resistance and transition resistance. Under the condition of a signal-to-noise ratio of 30 dB, the positioning error is only 0.26 km, which is about 70.5% less than traditional ELM; Under extreme conditions where the transition resistance increases to 300 Ω, the error remains at 0.31 km, significantly better than ELM's 0.72 km and KELM's 0.54 km, demonstrating strong environmental adaptability and robustness.

In summary, the KELM fault location method proposed by the paper based on BWO optimization and uncertainty estimation has successfully achieved the fusion of high accuracy, interpretability, and robustness, and can maintain reliable performance under complex working conditions such as severe noise interference and drastic impedance changes. Future work can further combine online learning and spatiotemporal feature fusion technology to achieve adaptive positioning and dynamic credibility evaluation of multi terminal DC systems, providing theoretical and methodological support for the next generation of intelligent protection and operation decision-making.

Funding

State Grid Corporation of China Technology Project (No.2020AAC03488).

Author contributions

Each author made significant individual contributions to this manuscript. Kai Yang: writing and performing surgeries; ,Haimo Wang , Bo Wu: data analysis and performing surgeries;Jinpeng Hao:article review and intellectual concept of the article.

Conflict of interest

The author declares that they have no competing interest.

Informed consent

Not applicable. This study did not involve human participants.

Ethical approval

The conducted research is not related to either human or animals use.

Consent to Participate

Not applicable.

Consent to publish

Not applicable.

Data availability statement

The datasets generated during and/or analysed during the current study are available from the corresponding author on reasonable request.

References

[1] Dashti, R., Daisy, M., Shaker, H. R., & Tahavori, M. (2018). Impedance-based fault location method for four-wire power distribution networks. IEEE Access, 6, 1342–1349. https://doi.org/10.1109/ACCESS.2017.2778427

[2] Zhang, C., Bi, T., Ren, Z., Thomas, D. W. P., & Sumner, M. (2020). Time-domain single-ended fault location method that does not need the information of the remote-end system. IET Generation, Transmission & Distribution, 14(7), 1234–1242. https://doi.org/10.1049/iet-gtd.2019.0647

[3] Yang, Y., Zhang, X., Liu, Y., & Sun, Y. (2023). Fault location method of multi-terminal transmission line based on CEEMDAN and double-ended ranging. Applied Sciences, 13(2), 1174. https://doi.org/10.3390/app13021174

[4] Iliyaeifar, M. M., & Hadaeghi, A. (2023). Extreme learning machine-based fault location approach for terminal-hybrid LCC–VSC–HVDC transmission lines. Electric Power Systems Research, 221, 109487. https://doi.org/10.1016/j.epsr.2023.109487

[5] Chandio, F. H., Bacha, S., Khan, B., Hussain, S. M. S., Lijana, D., & Ali, M. U. (2023). Control and protection of modular multilevel converter based high voltage direct current systems: A review. Energy Reports, 9, 7219–7243. https://doi.org/10.1016/j.egyr.2022.12.056

[6] Gharaghani, F., & Asadi, M. (2023). Modular multilevel converter–HVDC systems: A review on control, operation, and challenges. Electrical Engineering, 105, 1979–2000. https://doi.org/10.1007/s00202-023-01908-1

[7] Muniappan, M., & Vadivel, K. (2021). A comprehensive review of DC fault protection methods in voltage-source-converter based HVDC systems. Protection and Control of

Modern Power Systems, 6, 1–15. https://doi.org/10.1186/s41601-020-00173-9

[8] Panahi, M., Rabiee, A., Cherkaoui, R., & Abdelaziz, A. Y. (2021). Advances in transmission network fault location in modern power systems: Review, outlook and future works. IEEE Access, 9, 158599–158626. https://doi.org/10.1109/ACCESS.2021.3129838

[9] Orozco-Henao, C., Zamora-Méndez, A., Calle-González, C., & Meléndez, J. (2018). Adaptive impedance-based fault location algorithm for transmission lines. Applied Sciences, 8(9), 1563. https://doi.org/10.3390/app8091563

[10] Chandran, S., Kanakaraj, J., & Srinivasan, K. (2024). An extended impedance-based fault location algorithm in transmission lines using PMU phasors. IET Generation, Transmission & Distribution, 18(9), 5439–5452. https://doi.org/10.1049/gtd2.13086

[11] Zhang, M., Wang, D., Gao, H., Peng, F., & Gao, M. (2024). Novel traveling-wave fault location method for HVDC transmission lines based on wavefront frequency. Electric Power Systems Research, 229, 110598. https://doi.org/10.1016/j.epsr.2024.110598

[12] Deng, F., Xiao, S., Wang, S., Li, H., & Wang, Y. (2021). Travelling-wave fault location algorithm for LCC–MMC–MTDC hybrid transmission system based on Hilbert–Huang transform. International Journal of Electrical Power & Energy Systems, 138, 107863. https://doi.org/10.1016/j.ijepes.2021.107863

[13] Wang, Y., Wu, T., Zhang, B., & Ding, Y. (2021). Novel travelling wave fault location principle for VSC-HVDC transmission lines. Electric Power Systems Research, 196, 107226. https://doi.org/10.1016/j.epsr.2021.107226

[14] Falaghi, A., Haghifam, M. R., & Abedi, A. (2017). Recognition of travelling surges in HVDC transmission lines using wavelet entropy. Entropy, 19(1), 34. https://doi.org/10.3390/e19010034

[15] Kumar, H. K. P., Dash, R., Reddy, K. J., Atyam, N. R., & Mohapatra, B. (2025). High-resistance fault detection in direct current microgrids using Hilbert–Huang transform and vector-based ensemble optimized long short-term memory networks. Scientific Reports, 15, 97975. https://doi.org/10.1038/s41598-025-00977-5

[16] de Aguiar, E. P., de Jesus, D. C., Pereira, R. A., & Bretas, A. S. (2019). Fault location in power distribution systems using wavelet transform and unsynchronized measurements. The Journal of Engineering, 2019(18), 4948–4952. https://doi.org/10.1049/joe.2018.8555

[17] Chen, Y.-B., Cao, H.-S., Huang, C.-W., & Zhang, Z.-Y. (2024). Improving transmission line fault diagnosis based on ensemble empirical mode decomposition and power spectral entropy. Entropy, 26(9), 806. https://doi.org/10.3390/e26090806

[18] Shu, H., Zhang, L., Li, M., Zhao, W., & Li, Y. (2021). A detection method of high-impedance arcing fault for distribution networks based on complete ensemble empirical mode decomposition with adaptive noise and multi-scale singular value decomposition. IET Generation, Transmission & Distribution, 15(18), 2577–2588. https://doi.org/10.1002/2050-7038.12926

[19] Jing, L., Liu, Q., Liu, Y., & Zhang, Y. (2023). An improved arc-fault location method of direct-current distribution networks based on empirical mode decomposition and variational mode decomposition. Applied Sciences, 13(16), 9132. https://doi.org/10.3390/app13169132

[20] Yu, K., Wang, X., Jiang, L., Yang, C., & Zhang, X. (2024). Study on travelling-wave fault localization of transmission line based on NGO-VMD algorithm. Energies, 17(9), 2003. https://doi.org/10.3390/en17092003

[21] Zhang, W., & Wang, D. (2022). S-transform based travelling-wave directional pilot protection for hybrid LCC–MMC–HVDC transmission lines. Energies, 15(13), 4802. https://doi.org/10.3390/en15134802

[22] Poursaeed, A. H., Leviez, O., Liu, Y., & Litak, G. (2024). High-speed algorithm for fault detection and location in direct current transmission lines using the high-order synchrosqueezing transform. IET Generation, Transmission & Distribution, 18(29), 4259–4272. https://doi.org/10.1049/gtd2.13274

[23] Zhu, X., Zhang, D., Zhou, Z., & Fang, J. (2022). Novel wavefront detection and fault location method based on Hilbert–Huang transform for long HVDC transmission lines. Electric Power Systems Research, 210, 108054. https://doi.org/10.1016/j.epsr.2022.108054

[24] Fei, C., Qi, G., & Li, C. (2018). Fault location on high-voltage transmission line by applying support vector regression with fault signal amplitudes. Electric Power Systems Research, 160, 173–179. https://doi.org/10.1016/j.epsr.2018.09.006

[25] Akmaz, D., Mamiş, M. S., Arkan, M., & Tağluk, M. E. (2018). Transmission line fault location using travelling-wave frequencies and extreme learning machine. Electric Power Systems Research, 155, 1–7. https://doi.org/10.1016/j.epsr.2017.09.018

[26] Yue, Y., Liu, P., Zhou, Y., & Bao, T. (2023). Towards an optimal kernel extreme learning machine using the hybrid particle-swarm and butterfly optimization approach. Mathematics, 11(2), 382. https://doi.org/10.3390/math11020382

[27] Cai, Z., Li, J., Zhang, Y., & Hu, J. (2019). Evolving an optimal kernel extreme learning machine by using an improved grey wolf optimizer. Expert Systems with Applications, 125, 291–302. https://doi.org/10.1016/j.eswa.2019.01.079

[28] Chai, W., Li, C., Wang, J., & Sun, Z. (2023). GA-KELM: Genetic-algorithm-improved kernel extreme learning machine. Mathematics, 11(16), 3574. https://doi.org/10.3390/math11163574

[29] Xia, Y., Li, L., Deng, X., & Jiang, S. (2022). Coupled extreme learning machine and particle swarm optimization for regression problems. Engineering Applications of Artificial Intelligence, 113, 104989. https://doi.org/10.1016/j.engappai.2022.104989

[30] Yang, S., & Yee, K. (2024). Towards reliable uncertainty quantification via deep ensembles in multi-output regression task. Engineering Applications of Artificial Intelligence, 131, 107871. https://doi.org/10.1016/j.engappai.2024.107871

[31] Hudomalj, M., Trost, A., & Čampa, A. (2024). Traveling wave method for event localization and characterization of power transmission lines. Electric Power Systems Research, 232, 110382. https://doi.org/10.1016/j.epsr.2024.110382

[32] Johannesson, N., Rahmatian, M., & Leth Bak, C. (2019). Contribution of travelling wave propagation time to the speed of protection schemes. IET Generation, Transmission & Distribution, 13(22), 4959–4966. https://doi.org/10.1049/iet-gtd.2019.0344

[33] Huai, Q., Liu, K., & Hooshyar, A. (2021). Single-ended line fault location method for multi-terminal HVDC system based on optimized variational mode decomposition. Electric Power Systems Research, 194, 107054. https://doi.org/10.1016/j.epsr.2021.107054

[34] Jena, M. K., Pradhan, A. K., & Routray, A. (2017). Variational mode decomposition-based power system disturbance analysis using wide-area measurements. IET Generation, Transmission & Distribution, 11(15), 3724–3733. https://doi.org/10.1049/iet-gtd.2016.1827

[35] Deng, W. Y., Ong, Y. S., Tan, P. S., & Zheng, Q. H. (2016). Online sequential reduced kernel extreme learning machine. Neurocomputing, 174, 72–84.

https://doi.org/10.1016/j.neucom.2015.06.087

[36] Yu, X., Feng, Y., Gao, Y., Jia, Y., & Mei, S. (2021). Dual-weighted kernel extreme learning machine for hyperspectral imagery classification. Remote Sensing, 13(3), 508. https://doi.org/10.3390/rs13030508